Original Article
Prepared for Numerical Methods in Biomedical Eng
Submitted on September 5, 2014
Final revision submitted on February 21, 2015

Focal Cartilage Defect Compromises Fluid-pressure Dependent Load Support in the Knee Joint

Y. Dabiri and L. P. Li *

Department of Mechanical and Manufacturing Engineering, University of Calgary, Alberta, Canada

Graphical Abstract

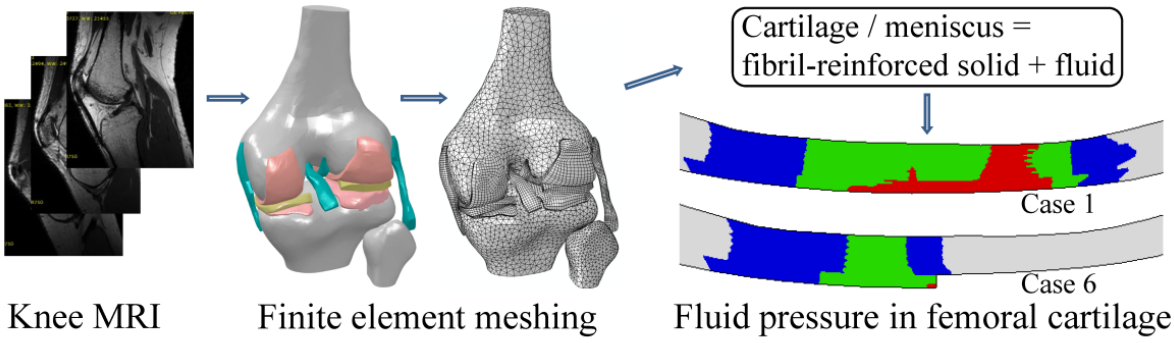

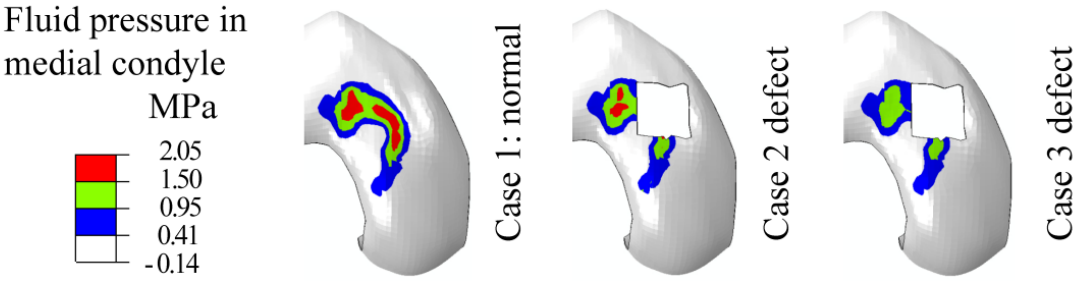

Abstract

A focal cartilage defect involves tissue loss or rupture. Altered mechanics in the affected joint may play an essential role in the onset and progression of osteoarthritis. The objective of the present study was to determine the compromised load support in the human knee joint during defect progression from the cartilage surface to the cartilage-bone interface. Ten normal and defect cases were simulated with a previously tested 3D finite element model of the knee. The focal defects were considered in both condyles within high load-bearing regions. Fluid pressurization, anisotropic fibril-reinforcement, and depth-dependent mechanical properties were considered for the articular cartilages and menisci. The results showed that a small cartilage defect could cause 25% reduction in the load support of the knee joint due to a reduced capacity of fluid pressurization in the defect cartilage. A partial-thickness defect could cause a fluid pressure decrease or increase in the *remaining underlying* cartilage depending on the defect depth. A cartilage defect also increased the shear strain at the cartilage-bone interface, which was more significant with a full-thickness defect. The effect of cartilage defect on the fluid pressurization also depended on the defect sites and contact conditions. In conclusion, a focal cartilage defect causes a fluid-pressure dependent load reallocation and a compromised load support in the joint, which depend on the defect depth, site and contact condition.

Keywords: Articular cartilage mechanics, Cartilage focal defect, Finite element analysis, Fluid pressure, Knee joint mechanics

Nomenclature

For the simplicity of description, these terms are defined with specific meaning. Force control: when a force is applied at a constant rate followed by creep; Displacement control: when a displacement is applied at a constant rate followed by relaxation; Short-term: the phase during which a force or displacement is being applied; Long-term: the time when significant relaxation or creep has occurred.

1. Introduction

Osteoarthritis (OA) is a leading cause of disability among the elderly, and the most prevalent joint disease in the USA [1]. OA may start from the surface of articular cartilage, and attack deeper layers until it reaches the bone [2,3]. Once the deep zone of cartilage is damaged, bone is exposed to the joint contact, leading to increased friction and reduced mobility of the joint. The knee joint has the highest prevalence of OA [4,5]. The cost of knee OA has been high and is expected to remain high for at least two decades because of the aging of our population [6].

OA is associated with perturbations in the composition and structure of articular cartilage [7,8,9]. Cartilage is composed of a collagen fiber network, proteoglycan matrix and a fluid [10]. For the convenience of description, cartilage is often divided into 3 distinct zones: superficial, middle, and deep zones [10]. The collagen fibers are mostly parallel to the surface in the superficial zone, randomly-oriented in the middle zone, and perpendicular to the cartilage-bone interface in the deep zone. These differences in fiber orientation and other zonal differences play important roles in the load support of cartilage and in the preservation of tissue integrity [3].

Fluid pressurization in cartilages and menisci is believed to play an essential role in the mechanics of the knee. It lubricates the joint and prevents cartilage matrix from excessive loading [11-13]. Fluid pressure contributes to load support of the joint at different scales during

different loading phases [14-16]. For example, the load applied to the knee joint during running produces a high fluid pressure whereas prolonged standing causes a continuous reduction in fluid pressure in cartilage and menisci. Substantial loading is transferred to the tissue matrices when the fluid pressure diminishes. The alteration in fluid pressurization is one of the symptoms in early OA [17,18]. However, the change of fluid pressure in situ as a function of loading time or disease process has not been adequately quantified in the literature due to experimental and modeling difficulties. In a recent study, the contact mechanics of the knee joint was investigated in the presence of cartilage degeneration with alterations in mechanical properties including fiber orientation [19]. That study, however, only took into consideration the short-term behavior of the knee joint. Moreover, it did not consider the fluid pressure in menisci and the full depth-dependent properties of cartilage.

Parameters such as defect depth, size, location, and altered tissue properties may influence the interplay between defect progression and fluid-pressure dependent load support [20-23]. Experimental studies encounter difficulties when investigating the effect of each of these parameters, because the consequence of each parameter is difficult to differentiate as they often evolve simultaneously. Numerical simulation is advantageous in determining the role of each parameter in the progression of OA [24,25]. The effect of defect size in the mechanics of the knee joint was reported using an elastic model [26,27] and thus the fluid pressure was not considered. The mechanics of cartilage defect has also been investigated with explants geometries [28] instead of realistic knee contact geometries.

The defect depth is a criterion to categorize the severity of a cartilage defect [20, 22]. For example, the International Cartilage Repair Society has a classification system for cartilage defect which is based on the depth-wise progression of the defect from the cartilage surface to

the cartilage-bone interface [20]. Therefore, the objective of the present study was to determine the alteration in fluid pressurization in articular cartilage and thus the compromised load support in the human knee joint during the depth-wise defect progression. We used realistic knee geometry reconstructed from magnetic resonance imaging (MRI) to clarify both short- and long-term load support of the knee in order to understand the degenerative mechanics of the joint.

2. Methods

2.1. Model Construction and Mesh

MRI of sagittal planes was obtained from a normal right knee of a male subject who was 27 years old with no injury. High resolution steady-state free precision sequences were used (distance between 2 neighboring images: 0.6 mm; size 22×22 cm, 512×512 pixels). The geometry of the knee joint was reconstructed using Mimics (Materialise, Leuven, Belgium). A short description of the method can be found in a review paper [29]. Briefly, the contrast of images was adjusted to improve appearance after the images were imported into Mimics. Segmentation was then performed to identify the boundaries for each tissue. A tool called "3D live wire" was used to identify the bone boundaries, while the tools "thresholding" and manual editing were used to identify the boundaries of cartilages and menisci. The geometries initially constructed were then refined using smoothing and wrapping tools to ensure the tissues were segmented precisely. Finally, an automatic smoothing procedure was performed to eliminate minor artifacts.

A finite element mesh was then generated, comprising of femur, femoral cartilage, menisci, tibial cartilage, and tibia [30,31]. Hexahedral pore pressure elements were used for the cartilaginous tissues, including 37537 elements for cartilages and 3424 for menisci. In order to

model the depth-wise defect progression, eight layers of elements were used for the femoral cartilage, resulting in thin elements (~0.25mm thick for most of these elements; smallest thickness 0.063mm, normally at the edge which is unloaded region; largest length 2.81mm).

2.2. Modeling Approaches and Boundary Conditions

The constitutive laws for the cartilaginous tissues, including all cartilages and menisci, were custom-coded with a user defined material model (UMAT in ABAQUS 6.10, Simulia, Providence, USA). The cartilaginous tissues were considered as fluid-saturated materials reinforced by a nonlinear fiber network, using a previously developed fibril-reinforced model of cartilage [14]. This previously validated constitutive model was used because it highlights fluid-pressure induced strong creep and relaxation [32,33]. The nonlinear tensile properties of the fiber network were explicitly implemented to account for the interplay of the nonlinear fibril reinforcement and fluid pressurization in the tissue [14]. The depth-varying tissue properties and fiber orientation of the femoral cartilage were also incorporated in the joint model as per a recent study [34]. The femur and tibia were modeled as linearly elastic, because the stiffness of the bones is 3 orders of magnitude higher than that of the cartilaginous tissues (thus their nonlinearity and poromechanical response are negligible when compared to that of cartilage and meniscus). The material properties are summarized in Table 1.

The contact mechanics of the knee was modeled using the surface-to-surface contact approach in ABAQUS. The penalty method was used to enforce the contact constraint. Six contact pairs were defined with 3 on the medial and 3 on the lateral sides. They modeled the actual contacts between femoral and tibial cartilage, femoral cartilage and menisci, and tibial cartilage and menisci. The femoral cartilage was fixed to the femur, and the tibial cartilage was

fixed to the tibia using the TIE CONTACT in ABAQUS. Menisci were fixed to the tibia at both ends to mimic the constraints applied by the posterior and anterior horns.

The boundary conditions were the same for all cases: the bottom of the tibia was fixed, and the top of femur was restrained from horizontal displacements. These constraints confined rigid-body motions. The fluid pressure boundary conditions were given as follows: the fluid pressure was zero on the free articular surface, whereas no fluid flow was assumed to cross the contact surface.

A comprehensive numerical verification has been previously performed on the joint model, including mesh convergence, sensitivity of material properties and parameters of numerical procedures [30,31,34].

2.3. Case Studies

Ten cases were investigated with finite element simulations in order to determine the effect of the defect site and depth, defect contact condition and loading protocol (Table 2).

Cartilage defects can be developed at different sites [23,35]. We focused on the depth-wise progression of defect in the medial condyle as it is more vulnerable to lesions than the lateral condyle [36-38]. Three types of cartilage defects were considered: (1) *Superficial defect* refers to tissue loss in the superficial zone only; (2) *Middle defect* refers to the loss in the superficial and middle zones; and (3) *Deep defect* refers to the complete loss in all 3 zones (full-thickness defect). A superficial defect in the lateral condyle was also examined for comparison with that in the medial condyle. The defect size was approximately 12×12 mm^2 (= 144 mm^2, Fig. 1), which was close to the mean defect size of 210 mm^2 observed from 1000 knee arthroscopies [39].

The contact conditions of the defect to its mating surface were also modeled. Although the tissue lost its thickness with the 3 types of defects, it is still possible for partial contact to occur

between the defect and its mating surface, as a result of very low stiffness and small thickness of cartilage (2-3mm tissue thickness comparing to $12\times12mm^2$ defect size). Patients tend to adjust their gait to ease pains when OA develops [40]. It is therefore also possible the defect would lose its contact with its mating surface. Hence, both scenarios, defect contact and non-contact, were modeled respectively. The extent of contact is determined automatically in ABAQUS as per the stress and strain state.

Two loading conditions were considered: (1) Ramp compression of 500 μm applied in 5s followed by relaxation; and (2) Ramp compressive force of 387.76 N applied in 5s followed by creep. This force was taken to be the same as obtained at the end of the 500 μm compression. The relaxation loading was used to understand the fundamental mechanism of the mechanical function of the knee joint, because the results from stress relaxation are easier to interpret. Creep loading was also simulated because creep is often considered a more realistic form of joint loading [41]. In either case, the compressive displacement or force was applied at the top of the femur while the knee was in full extension.

3. Results

For the same knee compression (displacement control), a decreased fluid pressure was observed in the *remaining underlying* cartilage in the case of the superficial defect as compared to the normal case (Fig. 1b vs 1a, at 5s). However, a raised pressure in the underlying cartilage was seen in the case of middle defect (Fig. 1c vs 1a). In these defect cases (Cases 2-4), a defect contact was assumed. On the other hand, the fluid pressure in the defective cartilage decreased with defect depth as expected (results not shown), when the defective tissue lost contact with its mating surface (Cases 6 & 7).

The short-term *surface* fluid pressure (Fig. 2a,b,c,d) in the vicinity of the defect region (in the unaffected tissue) decreased with the defect depth; a redistribution of the fluid pressure was more obvious when the defect was progressed to full-thickness. The long-term fluid pressure (Fig. 2e,f,g,h) experienced less alteration with the defect. Surprisingly, the alteration in the long-term pressure distribution was slightly more obvious with the middle defect (Fig. 2g). Furthermore, the fluid pressure in the lateral condyle was not obviously affected by the defect in the medial condyle (Fig. 1). Therefore, the results are shown for the medial condyle only in Fig. 2. The depth variation of the pressure was also altered with the defect (Fig. 3).

The reaction force of the affected joint could increase above or decrease below the normal value depending on the defect contact condition and relaxation time; the peak load in the joint varied over 25% with the cases (Fig. 4, displacement control). When the defect contact indeed occurred (Cases 2-4), the short-term reaction force was the highest in the case of middle defect, but the long-term reaction force reduced with the defect depth (Fig. 4a). When the defect contact did not occur (Cases 6-7), the reaction force was virtually the same for the 2 affected cases, which was also close to the reaction force predicted for Case 4 (Fig. 4b). These results also indicated that fluid pressure in cartilages and menisci could support roughly 2/3 of the joint load (Fig 4, short-term compares to long-term response).

A cartilage defect in the lateral condyle altered the fluid pressure more than a defect in the medial condyle (Fig. 5a,b,c). Two high pressure regions were produced in the lateral condyle due to the defect in that condyle (Fig.5c) as compared to one high pressure region in the normal case (Fig. 5a). For the cases of force control (Fig. 5d,e,f), the increase in the fluid pressure in the remaining underlying cartilage was more obvious than that of the displacement control, especially for the defect in the lateral condyle (Fig. 5f vs 5e or 5d).

The shear strain component in the cartilage-bone interface increased with the defect depth (Fig. 6). The superficial defect did not cause noticeable change in the shear strain. However, the middle and deep defects produced obvious changes in the shear strain both in magnitude and distribution. The location of peak shear strain moved towards the rim of the defect as the defect advanced to the deeper layer.

4. Discussion

A redistribution of the fluid pressure has been observed in the defect region and its vicinity (Figs. 1-3, 5-6), resulting in a load reallocation in the joint during fluid pressurization. Generally speaking, the load support of articular cartilage was weakened in the vicinity of the defect due to a reduced fluid pressure support in the tissue (Fig. 2). The remaining underlying cartilage at the defect, however, could be more pressurized (Fig. 1c vs 1a), when the defect was in contact with its mating surface. In the case of displacement control, a weakened load support meant a decreased fluid pressure in the vicinity of the defect, as compared to normal joint. Furthermore, the fluid pressure decreased with the defect depth (Fig. 2). In the case of force control, a weakened capacity in fluid pressurization required increased compression to raise the fluid pressure in the vicinity of the defect (Fig. 5d,e,f), in order to maintain the load support in the joint. Therefore, the creep and relaxation responses were reasonably related although they appeared different.

The load support of the knee joint, as indicated by the reaction force under a given compression, could be lowered by 25% due to the focal defect (Fig. 4). This means if the person is to maintain the same knee compression in the affected joint as in the normal joint, he/she must shift some load from the affected leg to the normal leg. The normal joint may then be somewhat

overloaded. Otherwise, the affected joint must be subjected to a substantially larger knee compression in order to maintain the same level load support in both joints. Therefore, cartilages and menisci in the affected joint may experience abnormally large deformation. Both scenarios may have detrimental impact on the future joint health.

The reduced capacity in fluid pressurization was not obviously seen in the case of creep (Fig. 5d,e,f) due to the same force being maintained in the normal and affected joints, as mentioned above. In other words, larger compressive displacement must be produced in the affected joint in order to support the same reaction force as that of the normal joint. In fact, a higher peak fluid pressure was seen in creep than in relaxation for the normal joint (Fig. 5d vs 5a), although the same force was applied in 5s in both creep and relaxation (Fig. 7). This phenomenon can be explained by the overall nonlinear response of the knee [42] and strain-rate dependent response of articular cartilage [32]. For the case of relaxation, the compression rate (displacement/time) was constant, corresponding to a lower loading rate (force/time) at the beginning and a higher loading rate at the end of the loading phase (Fig. 7). For the case of creep, however, the loading rate was constant during the loading phase, resulting in a higher compression rate at the beginning (but a lower compression rate at the end) of the loading phase as compared to the case of relaxation. The faster early compression produced a higher fluid pressure (as compared to the case of relaxation) during the early loading phase due to the strain-rate dependence of cartilage [32]. This higher fluid pressure did not have sufficient time to diminish although the compression was slowed down in the late loading phase. Therefore, we see a higher peak fluid pressure in creep than in relaxation even though the reaction forces were identical at the end of the loading phase.

As indicated above, the creep behavior is often more difficult to interpret than the relaxation behavior. Furthermore, creep modeling requires much more computing time than relaxation modeling (it took one month or longer computing time for a complete creep simulation). This is because a faster increasing fluid pressure in creep results in a slower numerical convergence and secondly, creep takes much longer time to reach its equilibrium [33]. On the other hand, a creep response can be qualitatively derived from the relaxation behavior, although they may look different (a mapping exists between the creep and relaxation responses). Therefore, the present study focused on the stress relaxation behavior of the knee joint while the creep response was also modeled.

The contact condition at the defect made a substantial difference in the load support of the knee joint although the defect size was small (Fig. 4). The remaining underlying cartilage at the defect still supported substantial loading when it was in contact with its mating surface (Fig. 4a, Cases 2 & 3 compared to Case 1). The reaction force in the affected knee was considerably lower, if the remaining underlying cartilage lost contact with its mating surface, even if the rest of the normal surfaces remained in contact (Fig. 4, Cases 6 & 7 vs Cases 2 & 3). Therefore, a slight gait adjustment by the OA patient would substantially change the load support in the joint. This result may be practically interesting, because people tend to adjust their gait to reduce pains after they developed OA [40].

The effect of cartilage defect on the fluid pressurization was also dependent on the defect site (Fig. 5). More results for the medial defect are presented in this paper, because the chosen region in the medial condyle is considered more vulnerable to the development of lesions [36-38].

The effect of cartilage defect on the fluid pressurization diminished with relaxation and creep time (Fig. 2e,f,g,h; Fig. 4), which was expected as fluid pressurization in the tissue decays with stress relaxation and creep. However, one would still expect the adverse impact of the defect on the long-term stresses and strains of the tissue matrix, as we see that the shear strains in the region increased with the defect depth (Fig. 6). This escalated shear strain may increase the chances of OA following a microfracture at the cartilage-bone interface [43-45], which agrees with previous studies on the importance of the tissue integrity [46,47]. The experimental measurements also showed time-dependent strains in the knee joint [48,49]. The time dependent mechanical response associated with fluid pressurization has gained increased attention in the joint modeling [49-54]. Published studies include modeling human knee joints using simplified axisymmetric geometries to reduce convergence difficulties and computing time [50,51]. The fluid pressure in human hip joints was also investigated [52,53]. Cartilage repair with a metal implant was simulated using a sheep knee model with a 3D simplified geometry and no meniscus [54]. All these studies have demonstrated, from different aspects, the essential role of fluid pressurization in the mechanical function of the normal and repaired joints.

The effects of focal cartilage defect on fluid pressure load support investigated here were somewhat similar to that of cartilage degeneration investigated previously [55]. Both caused the reduced capacity of fluid pressurization in the vicinity of the affected tissue; and the reductions were positively correlated to the depth of the defect or degeneration. However, a partial cartilage defect did not necessarily cause a fluid pressure reduction in the remaining underlying layers (Figs. 1 & 5f), as it occurred in cartilage degeneration. For example, when compared to the normal case, a degeneration advancing to the middle zone caused a reduced fluid pressure in the deep zone [55], but a defect advancing to the middle zone produced a higher fluid pressure in the

deep zone (Fig. 1c). Furthermore, a substantially compromised load support in the knee joint was found in the present study on the cartilage defect.

The major limitation of the present study was the use of simple physiological loadings, which were relatively small (< 400 N) and slowly applied to the joint (5 s). These loading protocols were used to avoid slow numerical convergence so the computing time was limited to approximately 2 weeks in most cases (4 CPUs on WestGrid high performance computing network). While the fluid pressures obtained were still low (0-4 MPa), they were close to the measured contact pressures (0-10 MPa) in the knee joints. Therefore, the results presented here are still practically interesting. Furthermore, the qualitative results would generally remain the same, if larger and faster loadings were used. On the other hand, varus/valgus rotations, flexion/extension, and internal/external torsions of the knee would substantially affect the contact mechanics of the knee joint, but the relevant topics were not within the scope of the present study. It must also be pointed out that the errors from geometrical reconstructions of the knee were not assessed in the present study. However, we believe such errors are minimal when advanced software such as Mimics is used with maximum care. The sensitivity of geometrical constructions has been studied by other groups [56].

In summary, focal cartilage defects substantially reduce the capacity of fluid pressurization in articular cartilage and subsequently compromise the load support in the joint. A redistribution of the fluid pressure occurs in the defect region and its vicinity, resulting in a load reallocation in the joint. The effect of cartilage defect on the load support of the joint diminished with relaxation and creep time, indicating the important role of the fluid pressurization that could support 2/3 of the joint load. Cartilage defects also increased the shear strain at the cartilage-bone interface. Furthermore, load-bearing characteristics of the knee joint deteriorate with the defect depth of

articular cartilage. The altered mechanics of the knee are also influenced by the sites of defects and the contact conditions in the defect regions. This compromised fluid-pressure dependent load support in the knee due to focal cartilage defect may have an implication on the onset and progression of OA.

Acknowledgments

Funding: the Natural Sciences and Engineering Research Council of Canada

Conflict of Interests: the authors have no conflict of interest to declare

Ethical approval: E-22593, University of Calgary, for the use of MRI of human subjects

References

[1] Peat G, Mccarney R, Croft P. Knee pain and osteoarthritis in older adults: a review of community burden and current use of primary health care. *Ann Rheum Dis* 2001; **60**: 91-97.

[2] Andriacchi TP, Mündermann A, Smith RL, Alexander EJ, Dyrby CO, Koo S. A framework for the in vivo pathomechanics of osteoarthritis at the knee. *Ann Biomed Eng* 2004; **32**: 447-457.

[3] Saarakkala S, Julkunen P, Kiviranta P, Mäkitalo J, Jurvelin JS, Korhonen RK. Depth-wise progression of osteoarthritis in human articular cartilage: investigation of composition, structure and biomechanics. *Osteoarthritis Cartilage* 2010; **18**: 73-81.

[4] Felson DT, Zhang Y. An update on the epidemiology of knee and hip osteoarthritis with a view to prevention. *Arthritis Rheum* 1998; **41**: 1343-1355.

[5] Oliveria SA, Felson DT, Reed JI, Cirillo PA, Walker AM. Incidence of symptomatic hand, hip, and knee osteoarthritis among patients in a health maintenance organization. *Arthritis Rheum* 1995; **38**: 1134-1141.

[6] Lethbridge-Cejku M, Schiller JS, Bernadel L. Summary health statistics for U.S. adults: National Health Interview Survey, 2002. *Vital Health Stat* 2004; **10**: 1-151.

[7] Guilak F, Ratcliffe A, Lane N, Rosenwasser MP, Mow VC. Mechanical and biochemical changes in the superficial zone of articular cartilage in canine experimental osteoarthritis. *J Orthop Res* 1994; **12**: 474-484.

[8] Mcdevitt CA, Muir H. Biochemical changes in the cartilage of the knee in experimental and natural osteoarthritis in the dog. *J Bone Joint Surg Br* 1976; **58**: 94-101.

[9] Stockwell RA, Billingham ME, Muir H. Ultrastructural changes in articular cartilage after experimental section of the anterior cruciate ligament of the dog knee. *J Anat* 1983; **136**: 425-439.

[10] Mow V, Ratcliffe A. Structure and function of articular cartilage and meniscus. In: Mow V, Hayes W (eds), *Basic orthopaedic biomechanics*. 2rd ed Lippincott-Raven, Philadelphia, 1997; 113-177.

[11] Ateshian GA, Hung CT. Patellofemoral joint biomechanics and tissue engineering. *Clin Orthop Relat Res* 2005; **436**: 81-90.

[12] Mccutchen CW. The frictional properties of animal joints. *Wear* 1962; **5**: 1-17.

[13] Walker PS, Dowson D, Longfield MD, Wright V. "Boosted lubrication" in synovial joints by fluid entrapment and enrichment. *Ann Rheum Dis* 1968; **27**: 512-520.

[14] Li LP, Buschmann MD, Shirazi-Adl A. The role of fibril reinforcement in the mechanical behavior of cartilage. *Biorheology* 2002; **39**: 89-96.

[15] Mow VC, Holmes MH, Lai WM. Fluid transport and mechanical properties of articular cartilage: a review. *J Biomech* 1984; **17**: 377-394.

[16] Vahdati A, Wagner DR. Finite element study of a tissue-engineered cartilage transplant in human tibiofemoral joint. *Comput Methods Biomech Biomed Eng* 2012; **15**: 1211-1221.

[17] Maroudas A. Balance between swelling pressure and collagen tension in normal and degenerate cartilage. *Nature* 1976; **260**: 808-809.

[18] Venn M, Maroudas A. Chemical composition and swelling of normal and osteoarthrotic femoral head cartilage. I. Chemical composition. *Ann Rheum Dis* 1977; **36**: 121-129.

[19] Mononen ME, Mikkola MT, Julkunen P, Ojala R, Nieminen MT, Jurvelin JS, Korhonen RK. Effect of superficial collagen patterns and fibrillation of femoral articular cartilage on knee joint mechanics-a 3D finite element analysis. *J Biomech* 2012; **45**: 579-587.

[20] Brittberg M, Winalski CS. Evaluation of cartilage injuries and repair. *J Bone Joint Surg Am* 2003; **85-A** Suppl 2: 58-69.

[21] Guettler JH, Demetropoulos CK, Yang KH, Jurist KA. Osteochondral defects in the human knee: influence of defect size on cartilage rim stress and load redistribution to surrounding cartilage. *Am J Sports Medicine* 2004; **32**: 1451-1458.

[22] Noyes FR, Stabler CL. A system for grading articular cartilage lesions at arthroscopy. *Am J Sports Med* 1989; **17**: 505-513.

[23] Seedholm BB, Takeda T, Tsubuku M, Wright V. Mechanical factors and patellofemoral osteoarthrosis. *Ann Rheum Dis* 1979; **38**: 307-316.

[24] Haut Donahue TL, Hull ML, Rashid MM, Jacobs CR. How the stiffness of meniscal attachments and meniscal material properties affect tibio-femoral contact pressure computed using a validated finite element model of the human knee joint. *J Biomech* 2003; **36**: 19-34.

[25] Ramaniraka NA, Terrier A, Theumann N, Siegrist O. Effects of the posterior cruciate ligament reconstruction on the biomechanics of the knee joint: a finite element analysis. *Clin Biomech* (Bristol, Avon) 2005; **20**: 434-442.

[26] Papaioannou G, Demetropoulos CK, King YH. Predicting the effects of knee focal articular surface injury with a patient-specific finite element model. *The Knee* 2010; **17**: 61-68.

[27] Peña E, Calvo B, Martínez MA, Doblaré M. Effect of the size and location of osteochondral defects in degenerative arthritis. A finite element simulation. *Comput Biol Med* 2007; **37**: 376-387.

[28] Duda GN, Maldonado ZM, Klein P, Heller MO, Burns J, Bail H. On the influence of mechanical conditions in osteochondral defect healing. *J Biomech* 2005; **38**: 843-851.

[29] Kazemi M, Dabiri Y, Li LP. Recent advances in computational mechanics of the human knee joint. *Computational and Mathematical Methods in Medicine* 2013, Article ID 718423, 27 pages, doi: 10.1155/2013/718423.

[30] Gu KB, Li LP. A human knee joint model considering fluid pressure and fiber orientation in cartilages and menisci. *Med Eng Phys* 2011; **33**: 497-503.

[31] Kazemi M, Li LP, Savard P, Buschmann MD. Creep behavior of the intact and meniscectomy knee joints. *J Mech Behav Biomed Mater* 2011; **4**: 1351-1358.

[32] Li LP, Herzog W. Strain-rate dependence of cartilage stiffness in unconfined compression: the role of fibril reinforcement versus tissue volume change in fluid pressurization. *J Biomech* 2004; **37**: 375-382.

[33] Li LP, Korhonen RK, Iivarinen J, Jurvelin JS, Herzog W. Fluid pressure driven fibril reinforcement in creep and relaxation tests of articular cartilage. *Med Eng Phys* 2008; **30**: 182-189.

[34] Dabiri Y, Li LP. Influences of the depth-dependent material inhomogeneity of articular cartilage on the fluid pressurization in the human knee. *Med Eng Phys* 2013; **35**: 1591-1598.

[35] Bae WC, Payanal MM, Chen AC, Hsieh-Bonassera ND, Ballard BL, Lotz MK, Coutts RD, Bugbee WD, Sah RL. Topographic Patterns of Cartilage Lesions in Knee Osteoarthritis. *Cartilage* 2010; **1**: 10-19.

[36] Biswal S, Hastie T, Andriacchi TP, Bergman GA Dillingham, MF, Lang P. Risk factors for progressive cartilage loss in the knee: a longitudinal magnetic resonance imaging study in forty-three patients. *Arthritis Rheum* 2002; **46**: 2884-2892.

[37] Tandogan RN, Taşer O, Kayaalp A, Taşkiran E, Pinar H, Alparslan B, Alturfan A. Analysis of meniscal and chondral lesions accompanying anterior cruciate ligament tears: relationship with age, time from injury, and level of sport. *Knee Surg Sports Traumatol Arthrosc* 2004; **12**: 262-270.

[38] Temple MM, Bae WC, Chen MQ, Lotz M, Amiel D, Coutts RD, Sah RL. Age- and site-associated biomechanical weakening of human articular cartilage of the femoral condyle. *Osteoarthritis Cartilage* 2007; **15**: 1042-1052.

[39] Hjelle K, Solheim E, Strand T, Muri R, Brittberg M. Articular cartilage defects in 1,000 knee arthroscopies. *Arthroscopy* 2002; **18**: 730-734.

[40] Kaufman KR, Hughes C, Morrey BF, Morrey M, An KN. Gait characteristics of patients with knee osteoarthritis. *J Biomech* 2001; **34**: 907-915.

[41] Athanasiou KA, Rosenwasser MP, Buckwalter JA, Malinin TI, Mow VC. Interspecies comparisons of in situ intrinsic mechanical properties of distal femoral cartilage. *Journal of Orthopaedic Research* 1991; **9**: 330-340.

[42] Li LP, Gu KB. Reconsideration on the use of elastic models to predict the instantaneous load response of the knee joint. *Proc Inst Mech Eng H – Journal of Engineering in Medicine* 2011; **225**: 888-896.

[43] Burr DB, Radin EL. Microfractures and microcracks in subchondral bone: are they relevant to osteoarthrosis? *Rheum Dis Clin North Am* 2003; **29**: 675-685.

[44] Radin EL, Rose RM. Role of subchondral bone in the initiation and progression of cartilage damage. *Clin Orthop Relat Res* 1986; **213**: 34-40.

[45] Vener MJ, Thompson RC, Lewis JL, Oegema TR. Subchondral damage after acute transarticular loading: an in vitro model of joint injury. *J Orthop Res* 1992; **10**: 759-765.

[46] Setton LA, Zhu W, Mow VC. The biphasic poroviscoelastic behavior of articular cartilage: role of the surface zone in governing the compressive behavior. *J Biomech* 1993; **26**: 581-592.

[47] Shirazi R, Shirazi-Adl A, Hurtig M. Role of cartilage collagen fibrils networks in knee joint biomechanics under compression. *J Biomech* 2008; **41**: 3340-3348.

[48] Hosseini A, Van de Velde SK, Kozanek M, Gill TJ, Grodzinsky AJ, Rubash HE, Li G. In-vivo time-dependent articular cartilage contact behavior of the tibiofemoral joint. *Osteoarthritis Cartilage* 2010; **18**: 909-916.

[49] Halonen KS, Mononen ME, Jurvelin JS, Toyräs J, Salo J, Korhonen RK. Deformation of articular cartilage during static loading of a knee joint – Experimental and finite element analysis. *J Biomech* 2014; **47**: 2467-2474.

[50] Adeeb SM, Sayed Ahmed EY, Matyas J, Hart DA, Frank CB, Shrive NG. Congruency effects on load bearing in diarthrodial joints. *Comput Methods Biomech Biomed Eng* 2004; **7**: 147-157.

[51] Guo H, Maher SA, Spilker RL. Biphasic finite element contact analysis of the knee joint using an augmented Lagrangian method. *Medical Eng Phys* 2013; **35**: 1313-1320.

[52] Li J, Hua X, Jin Z, Fisher J, Wilcox RK. Influence of clearance on the time-dependent performance of the hip following hemiarthroplasty. *Medical Eng Phys* 2014; **36**: 1449-1454.

[53] Fietz K. Towards a finite element model for fluid flow in the human hip joint. MSc thesis (supervisors: Nackenhorst U, Markert B), Leibniz Universität Hannover, Germany, 2013.

[54] Manda K, Eriksson A. Time-dependent behavior of cartilage surrounding a metal implant for full-thickness cartilage defects of various sizes: a finite element study. *Biomech Model Mechanobiol* 2012; **11**: 731-742.

[55] Dabiri Y, Li LP. Altered knee joint mechanics in simple compression associated with early cartilage degeneration. *Comput Math Methods Med* 2013; Article ID 862903, 11 pages, doi:10.1155/2013/862903.

[56] Li G, Lopez O, Rubash H. Variability of a three dimensional finite element model constructed using magnetic resonance images of a knee for joint contact stress analysis. *Journal of Biomechanical Engineering* 2001; **123**: 341–346.

Table 1. Material properties for all tissues (Modulus: MPa; Permeability: 10^{-3}mm^4/Ns). The *x* is the primary fiber direction, i.e. the split-line direction for the superficial zone, the depth direction for the deep zone for articular cartilage, and the circumferential direction for the meniscus. The *y* and *z* are normal to the primary fiber direction. The properties are the same in the *y* and *z* directions. For simplicity, the superficial, middle and deep zones were taken to be approximately 25%, 50% and 25% of the cartilage thickness [34]. The permeability is defined in Darcy's law. The coefficient of surface friction is 0.02.

Tissue		Fibrillar matrix		Nonfibrillar matrix		Permeability	
		E_x	E_y or E_z	E_m	υ_m	k_x	k_y or k_z
Femoral cartilage	Deep zone	$3 + 1600\varepsilon_x$	$0.9 + 480\varepsilon_{y/z}$	0.80	0.36	1.0	0.5
	Middle zone	$2 + 1000\varepsilon_x$	$2 + 1000\varepsilon_{y/z}$	0.60	0.30	3.0	1.0
	Superficial zone	$4 + 2200\varepsilon_x$	$1.2 + 660\varepsilon_{y/z}$	0.20	0.16	1.0	0.5
Tibial cartilage		$2 + 1000\varepsilon_x$	$2 + 1000\varepsilon_{y/z}$	0.26	0.36	2.0	1.0
Menisci		28	5	0.50	0.36	2.0	1.0
Bones		E = 5000		υ = 0.30			

Table 2. Ten cases investigated in the present study. Three cartilage conditions were considered: normal cartilage, defects in the medial and lateral condyles, respectively; three defect depths were also assumed for the medial condyle defect: the defect in the superficial zone only, the defect up to the middle zone and the defect up to the deep zone. Both force and displacement controls were simulated. In Cases 6 and 7, no contact was assumed between the defect and its mating surface.

Loading conditions	Normal cartilage		Medial condyle defect			Lateral condyle defect
			Superficial	Middle	Deep	Superficial
Displacement control (Relaxation)	**Case 1**	Defect contact	**Case 2**	**Case 3**	**Case 4**	**Case 5**
		No defect contact	**Case 6**	**Case 7**		
Force control (Creep)	**Case 8**	Defect contact	**Case 9**			**Case 10**

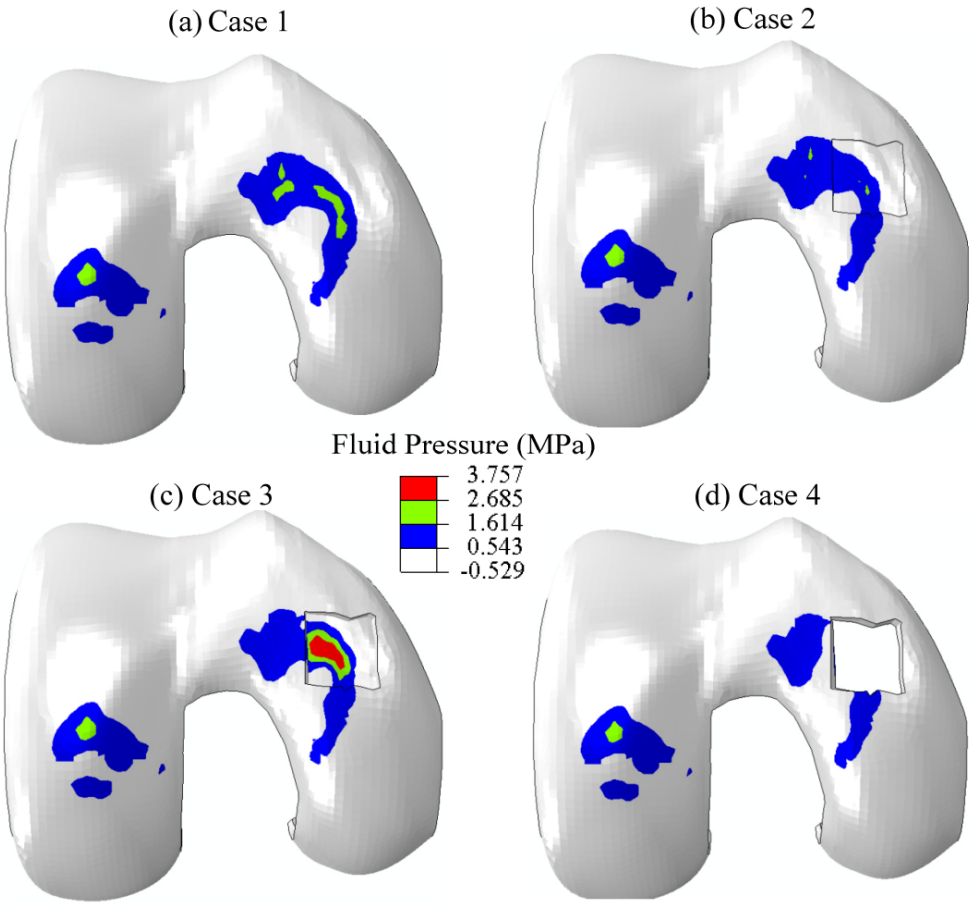

Fig. 1. Surface fluid pressure in the femoral cartilage at 500μm knee compression prior to relaxation (at 5s), showing for the layer of 1/16 depth. For cases of the partial-thickness defect, the fluid pressure in the *remaining underlying* cartilage is shown for the new surface layer, i.e. at the 5/16 (Case 2) and 13/16 (Case 3) depth respectively (shown in the insets). *The depth is normalized by the thickness of cartilage prior to defect* (0 = articular surface; 1 = cartilage/bone interface). This is an inferior view of the right knee, i.e. the medial condyle is on the right. Case 1: Normal cartilage; Case 2: Superficial defect; Case 3: Middle defect; Case 4: Deep defect.

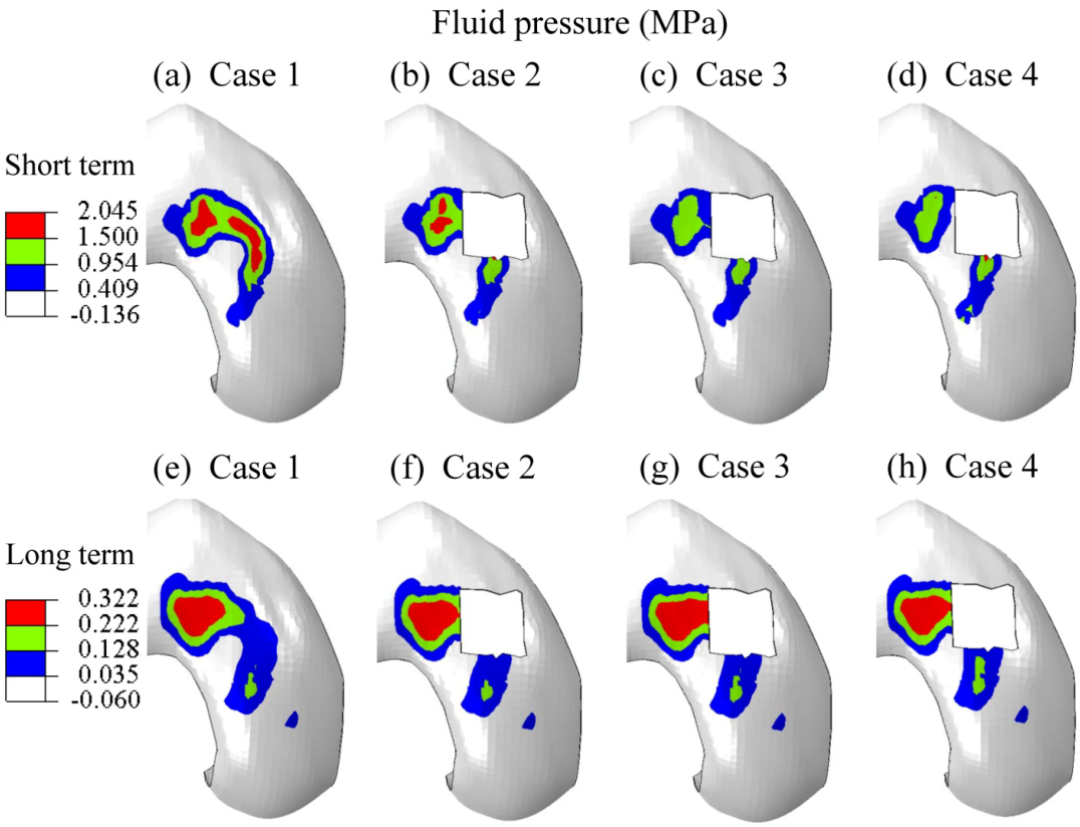

Fig. 2. Surface fluid pressure in the medial condyle at 500μm knee compression prior to relaxation (Short term: 2a, 2b, 2c, 2d) and at 1000s relaxation (Long term: 2e, 2f, 2g, 2h). Defect contact was assumed in the 3 affected cases (Cases 2-4). The defect region is blanked out.

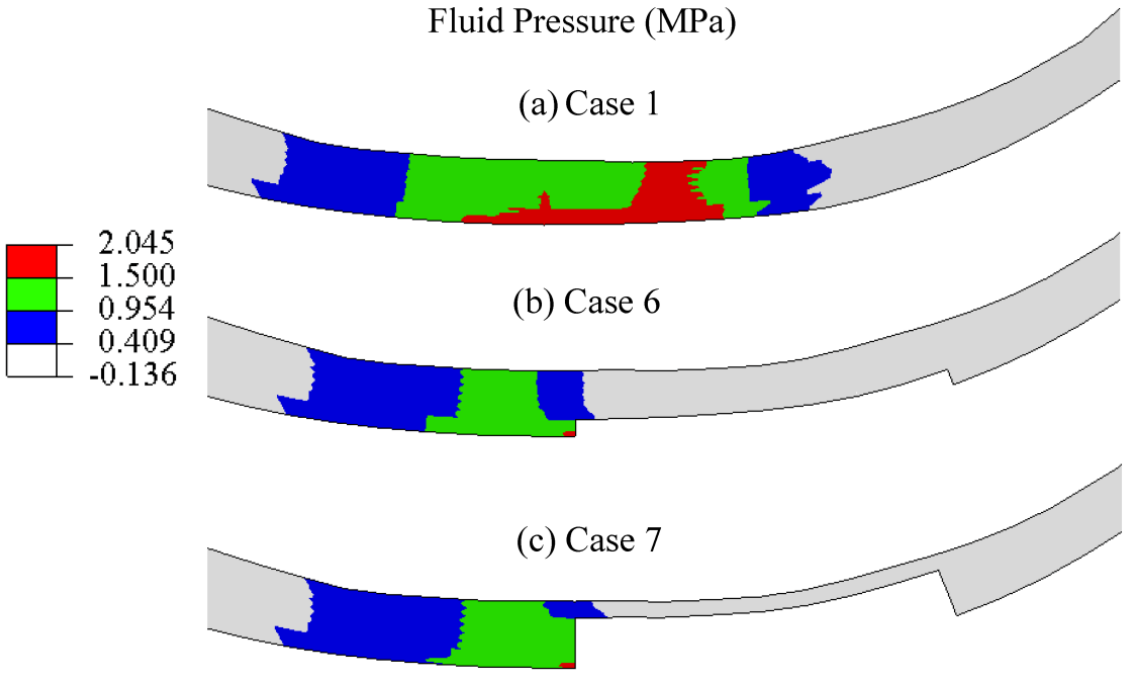

Fig. 3. Fluid pressure in a sagittal plane of the femoral cartilage at 500μm compression prior to relaxation, shown for the high load-bearing region of the medial condyle. (a) Normal cartilage (Case 1), (b) Superficial defect (Case 6, no defect contact), and (c) Middle defect (Case 7, no defect contact). The anterior side is on the left.

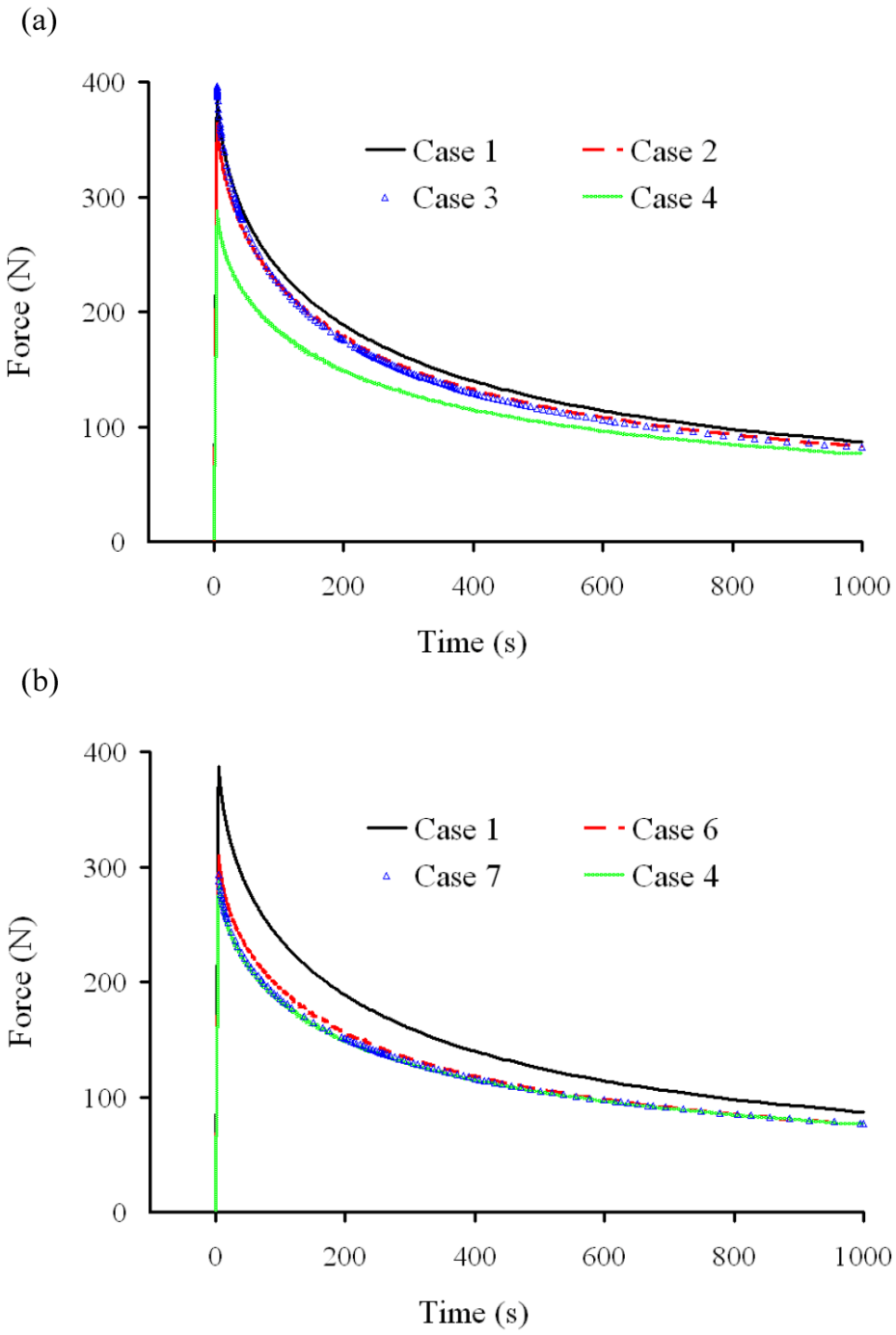

Fig. 4. Reaction force in the knee as a function of time for the ramp compression of 500μm followed by relaxation. (a) Defect contact was assumed in the defect cases (peak forces are Case 1: 387.8; Case 2: 363.6; Case 3: 396.3; Case 4: 288.1N); and (b) No defect contact was assumed in Cases 6 and 7 (peak forces are Case 6: 309.5; Case 7: 293.6N). These defect cases are all medial condyle defects.

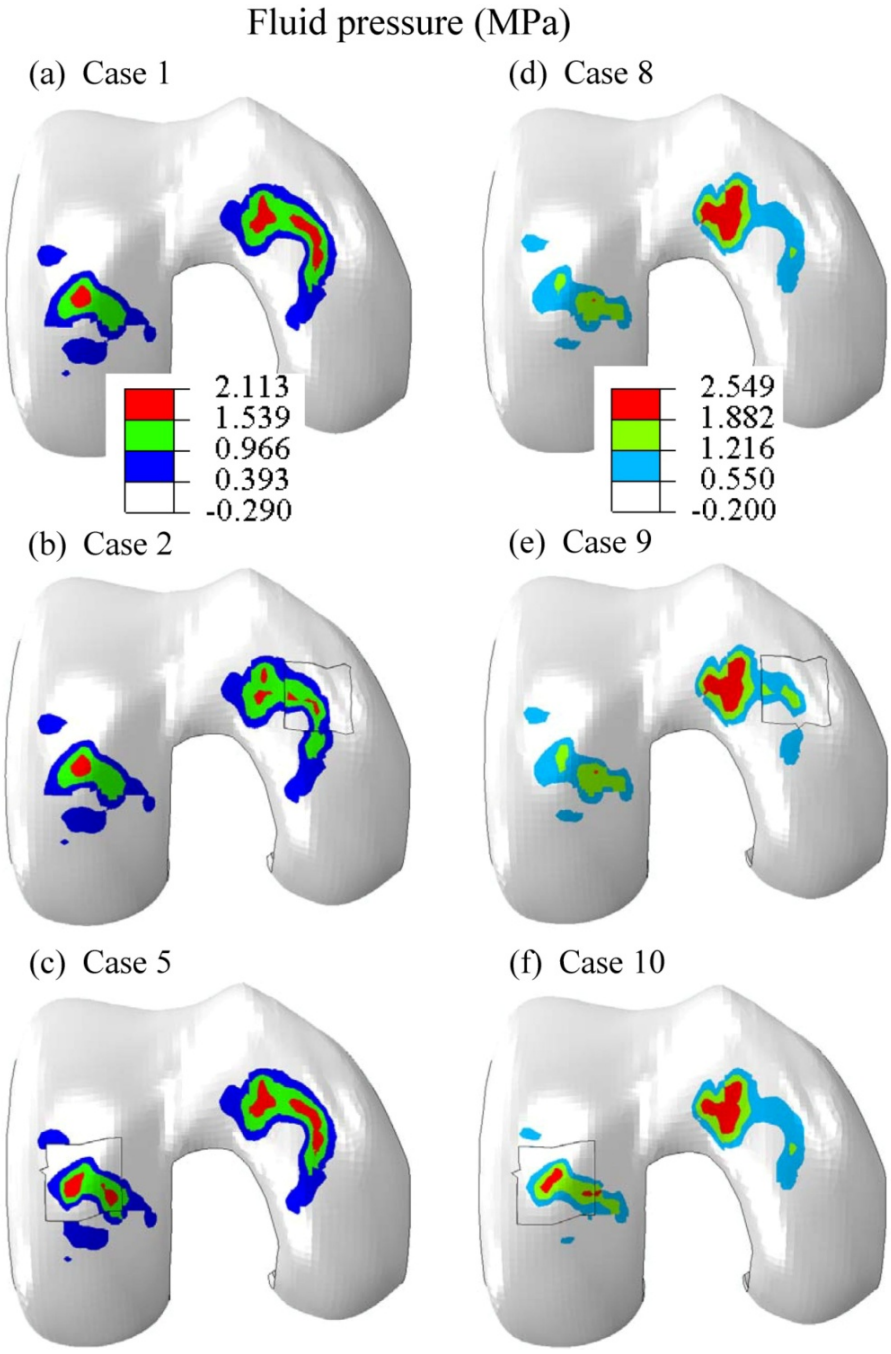

Fig. 5. Surface fluid pressure in the femoral cartilage at 500μm ramp compression prior to relaxation (5a, 5b, 5c) and at 387.76N ramp compressive loading prior to creep (5d, 5e, 5f). For the affected cases, which are all superficial defects, the fluid pressure in the defect region is shown for the new surface layer, i.e. at the depth of 5/16. Defect contact was assumed in the 4 affected cases including medial condyle defect (5b, 5e) and lateral condyle defect (5c, 5f).

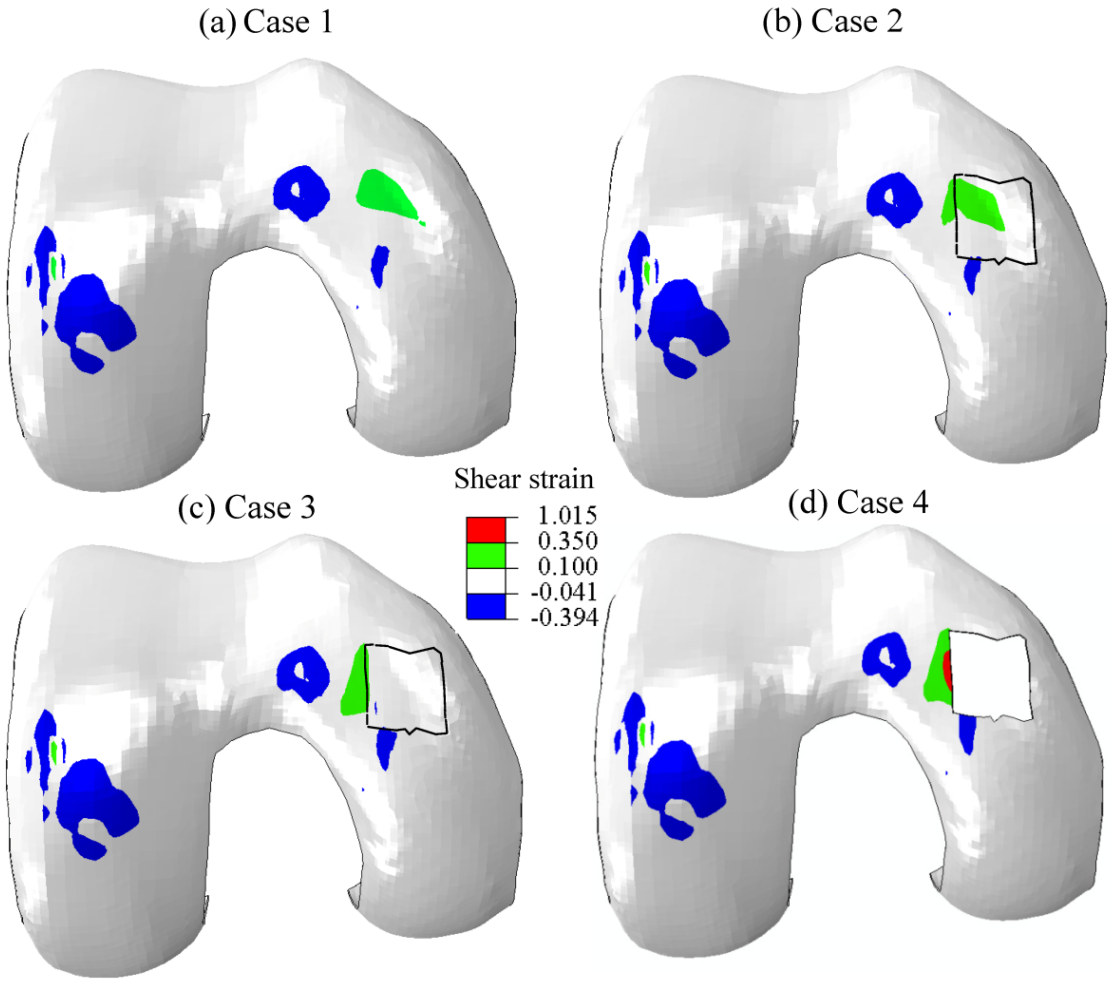

Fig. 6. Shear strain in the deepest cartilage layer during late relaxation of 500μm knee compression (at 1000s). (a) Normal cartilage, (b) Superficial defect, (c) Middle defect, and (d) Deep defect. Defect contact was assumed in the affected cases (Cases 2-4). The medial condyle is on the right.

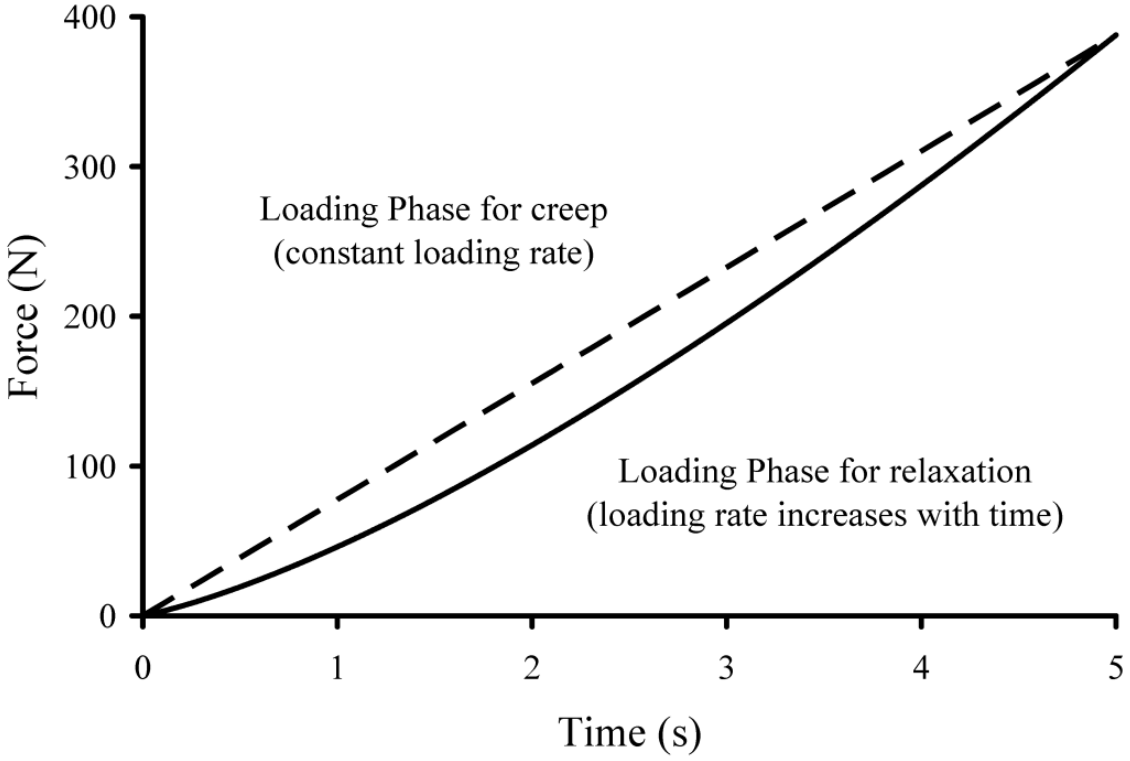

Fig. 7. Reaction forces in the knee as functions of time during the loading phase for the cases of creep and stress relaxation. In the case of creep (dash line), the loading rate was constant (force control); while in the case of relaxation (solid curve), the knee joint experienced an increasing loading rate (the slope of the curve increases with time) due to nonlinear behavior. The curve for the case of relaxation was taken from Fig. 4 for the normal joint (Case 1).